2020-01-01

A High-Temperature Valve Design for a Solid Oxide Fuel Cell/Gas Turbine Hybrid System

Cynthia Morales
University of Texas at El Paso

A HIGH-TEMPERATURE VALVE DESIGN FOR A SOLID OXIDE/FUEL CELL GAS TURBINE HYBRID SYSTEM

CYNTHIA MORALES

Master's Program in Mechanical Engineering

APPROVED:

Norman D. Love, Jr., Ph.D., Chair

Arifur R. Khan, Ph.D.

Tzu-Liang (Bill) Tseng, Ph.D.

Stephen L. Crites, Jr., Ph.D.
Dean of the Graduate School

Dedication

This work is dedicated to my loving family

A HIGH-TEMPERATURE VALVE DESIGN FOR A SOLID OXIDE FUEL CELL/GAS TURBINE HYBRID SYSTEM

by

CYNTHIA MORALES, B.S.M.E.

THESIS

Presented to the Faculty of the Graduate School of

The University of Texas at El Paso

in Partial Fulfillment

of the Requirements

for the Degree of

MASTER OF SCIENCE

Department of Mechanical Engineering

THE UNIVERSITY OF TEXAS AT EL PASO

August 2020

Acknowledgements

I would like to begin by thanking my advisor Dr. Norman Love for his mentorship, patience, continuous support and belief in my skills and abilities. It has been a tough journey in which he has helped me to get the best out of me even if the situation looks impossible. I take from him his knowledge, advice and hard work ethic to pass on to fellow classmates, siblings, friends and co-workers. Thank you to Department of Energy for funding and supporting this project to develop new ideas for the future. I would also like to thank the Energy Team but especially Karen Sida, Ariztbe Valladolid and Daniela Morales for always moving this project forward and not allowing it to collapse.

I would also like to thank my family for their love, patience, support and precious advice when I need it the most. Thank you to Dr. Arifur Khan and Dr. Tzu-Liang Tseng for their time and interest in the thesis.

Abstract

Systems containing high heat generation require thermal management, especially in a solid oxide fuel cell gas turbine (SOFC/GT) hybrid system [1]. The startup of each system in a standalone configuration may be a trivial approach, but when coupled together, different dynamics are experienced. The SOFC/GT provide high theoretical efficiency due to the ability to recover the extra heat produced by the fuel cell (FC) to drive the gas turbine (GT). After recovering the energy recuperated in the GT, the exhaust gas heats the cathode inlet flow to the FC which is an advantage during nominal operation of the cycle but not during startup. During startup of the SOFC/GT system, the turbine needs to startup as fast as possible where the surge is avoided and slow enough that the high heat of exhaust gas does not thermally shock the FC.

Therefore, with a bypass valve integrated in this system it will help to control the air flow going towards the FC and GT. Although a high temperature valve can be custom design by any company, it can result very expensive. However, self-designing the valve has also led to many challenges by examining the properties of materials that can stand very high temperatures. Other challenges are the design of the valve built-in to the actual SOFC/GT hybrid system, testing in high temperatures, analyzing the composites' displacement, tolerance at different voltage levels, and identifying how much flow rate will flow through the pipe or get blocked.

Table of Contents

List of Tables

List of Figures

List of Illustrations

Chapter 1

INTRODUCTION AND BACKGROUND

This study proposes a high temperature, and pressure bypass valve to control the airflow going towards a turbine and heat exchanger during the startup of a SOFC/GT system [1,2]. To control the high temperatures exhausted from the post-combustor, a bypass valve will be placed before the heat exchanger to regulate the airflow going to the fuel cell and avoid thermal stress on the material. However, during startup, the turbine also needs to achieve a nominal speed of 40,500 rpm and once it is achieved the valve must stay partly open to keep a certain amount of heat flowing through to keep the system operating. The main objective of this project is to design and develop a bypass valve capable of withstanding high temperatures, and pressure airflow during the startup of a cyber-physical SOFC/GT hybrid system located in the U.S. Department of Energy's National Energy Technology Laboratory (NETL) in Morgantown, WV.

1.1 DESIGN BACKGROUND

High-temperature valves are hard to find in the market due to its high complexity of having a design that can withstand very high temperature ranges. Many companies or laboratories can have a custom design but can result costly. Hence, NETL's goal is to open new development ideas in this research area since it could become very efficient for a hybrid system. New development ideas for this research helps scientists to investigate a variety of valves to widen their knowledge for new applications and at the same time it saves them money. Many valves used in piping were studied to find different types of designs held out in the market [3].

The attain of this research was to determine which valve is useful for the design to be modernized. An innovation for the valve was to integrate a composite inside the pipe acting as a

valve working as a gate. In order to perform this task, the design of the valve was first considered to visualize how the composite was going to be positioned inside the pipe. Finally, the gate valve was chosen to be the initiative of the design.

1.2 High Temperature Valves in the Market

There were six different types of valves found in the market designed for high temperatures. These companies were not found in the United States of America, but only in Italy and Germany. Shown below is a table listing the valves found along with their design parameters and other information.

Table 1.1: Different Types of Valves in the Market

Type of Valve	Company	Temperature Range	Material
Floating Ball	Erreesse	551°C to 1100°C	Specific metal alloys
Trunnion Ball	Erreesse	551°C to 1100°C	Specific metal alloys
Rectangular	Jasta	-100°C to +1100°C	Steel/Stainless steel
Weld-in EDR I	Jasta	-100°C to +1100°C	Steel/Stainless steel
Weld-in EDR II	Jasta	-100°C to +1100°C	Steel/Stainless steel
Weld-in EDR III	Jasta	-100°C to +1100°C	Steel/Stainless steel

These valves are used for extreme temperature range, so specific alloys are studied for high temperature conditions for an appropriate valve construction. Custom designs are offered for the individuals need depending on the application of the actuator. Drying and dust extractors, gas turbines, heat treatment, cement factories and high temperature furnace construction are some application areas these valves are used for. However, these valves need to be operated manually which is why this project proposes a different type of valve. A goal of this project is to protect the individual operating the valve due to high temperature exposure.

1.3 DoE HYPER Facility

Figure 1.3.1 illustrates the system concept of a hybrid FC/GT cycle that combines heat and hybrid power system. The anode, electrolyte and cathode block represent the SOFC stack in which methane is reformed and becomes oxidized for power generation. The reformer residuals flow into a post-combustor for additional power generation. However, the use of a pre-combustor in front of a fuel cell may cause H_2O going into cathode, which would accelerate the degradation of the fuel cells. Thus, an additional heat exchanger is proposed to warm up the cathode airflow, in which a bypass pipe with valve is needed for startup. Figure 1.3.1 circled in yellow shows the location of the heat exchanger and bypass pipe proposed for this project.

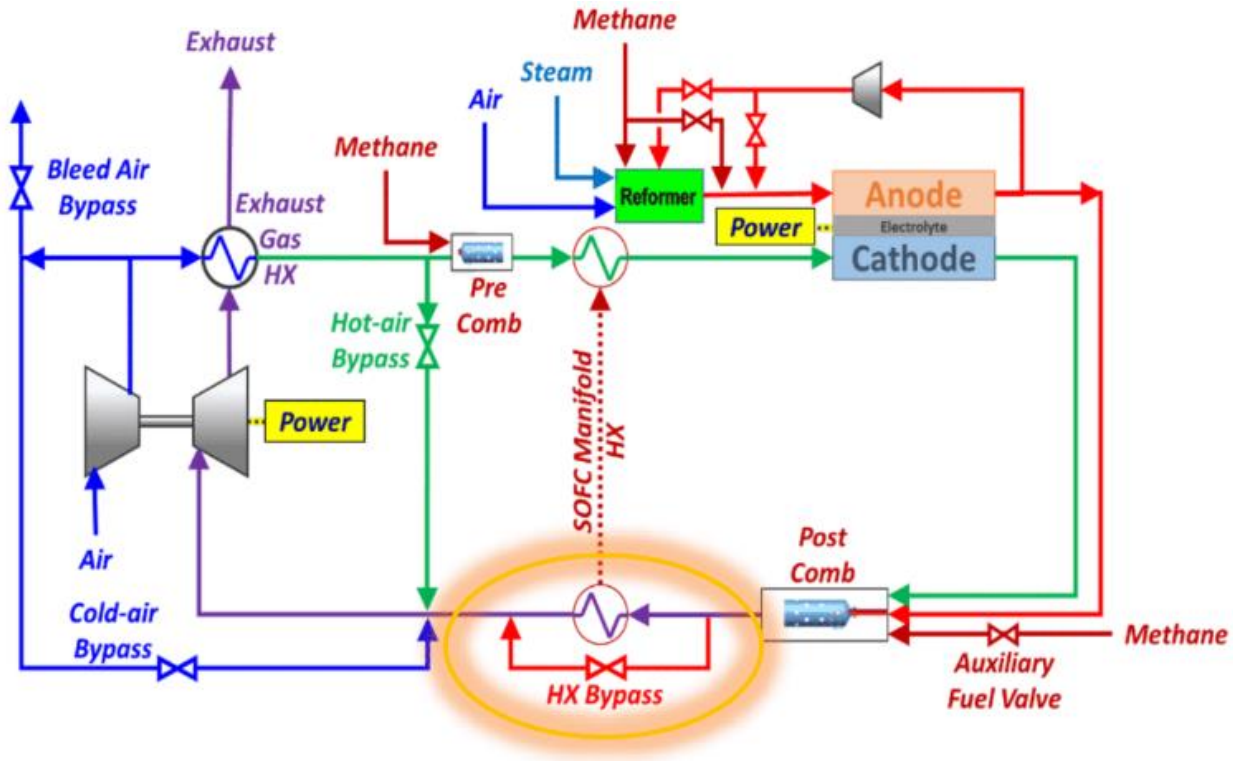

Figure 1.3.1: Hybrid Performance (HYPER) Project Diagram

The bypass valve controls the airflow directed to the turbine and the fuel cell. The bypass valve is represented in figure 1.3.2 illustrating the position of the piezoelectric. When the piezoelectric is subjected to voltage it will bend; the piezoelectric remains in a flat position when no voltage is used. The application of the piezoelectric material in the bypass valve is explained further ahead.

Figure 1.3.2: Bypass valve representation for HYPER facility

1.4 HIGH TEMPERATURE MATERIALS

The most significant task is to explore on the material of the valve, especially looking into a flexible composite. It is important to consider the curie and melting temperature of each composite. If the temperature of the valve exceeds the material's curie temperature, then this composite would lose all its electromagnetic properties and would not function correctly. Many composite materials were analyzed, however, the shape memory alloy (SMA) offered the best mechanical properties for the valve. The three studied SMA are the following: nickel titanium (Ni-Ti), nickel titanium cobalt (Ni-Ti-Co) and nickel titanium copper (Ni-Ti-Cu) [4].

Most of the materials considered for this project are smart materials. The next sections discuss more in depth what types of materials were considered and explains what their functions are. However, SMA and MFC were the most intriguing materials to work with and analyze. The

material for the actuator used inside the pipe is the most important job to be determined in the design. The selection of the material will help accomplish the mechanism of the valve acting in a hybrid system at extremely high temperatures. This chapter gives a brief explanation on what types of materials were sought and how they have been applied in research areas and in the industry. The next materials discussed are in the same order as this research was being constructed.

1.5 Lithium Niobate Theory and Applications

Lithium niobate is a high temperature piezoelectric with a curie temperature of 1050°C and a melting point of 1250°C [11]. It can be used for a variety of applications like sensors, mobile phones, optical and some others. Lithium niobate was discovered by Matthias and Remeika in 1949 to speed the need on technologies for data storage, biomedical and defense applications in the industry [12]. This piezoelectric offer great mechanical properties that meet the design requirements in high temperatures, but it is not flexible enough to be used as an actuator. Table 1.2 display different types of piezoelectrics along with its curie temperature, thus assuring lithium niobate can tolerate high temperatures [12-16].

Table 1.2 Types of Piezoelectric

Material	Transition Temperature, °C	Transition Type
Bismuth Titanate, Bi_3TiO_9	670	Curie Temperature
Lithium Niobate, $LiNbO_3$	1210	Curie Temperature
Lithium Tantalate, $LiTaO_3$	634	Curie Temperature
Lead Titanate, $PbTiO_3$	490	Curie Temperature
Lead Zirconate Titanate, *PZT*	350	Curie Temperature

Nowadays Lithium Niobate is mostly used for photonic crystal applications which are optical materials to control light flow. These types of applications also include lasers, non-linear optics, optical communications, optical memories, and diffractive optics [21].

Yongfa Kong et al wrote about the recent progress in lithium niobate [33]. Studies show that lithium niobate along with magnesium have been considered the material with best optical damage resistance. However, recent results designate that lithium niobate and zirconium have a much higher optical damage resistance in visible region, and in the ultraviolet. Lithium niobate is considered one of the most important synthetic crystals. Yang He et al studied the lithium niobate microring resonators [34], in which engineering of group-velocity dispersion (GVD) is crucial for most important nonlinear photonic applications. Throughout many research studies it is approved that lithium niobate shows great material properties with prodigious potential for countless applications.

1.6 Macro Fiber Composite Theory and Applications

A Macro Fiber Composite (MFC) is a smart material that was invented by NASA's Langley Research Center in 1999 which is still being developed for aerospace structures at NASA [5]. It is a low-cost piezoelectric device that reduces vibrations, deflections in composite beams, and noise. Some interesting benefits this smart material offers are flexibility, durability, lightweight, sensing and among others. An important benefit that the MFC operates is that it can elongate (d33 effect actuator) and contract (d31 effect actuator) [7]. The MFC is built of ceramic fibers and can be attached to a substrate to have a greater curvature as shown in figure 1.6.1 working like a monomorph actuator.

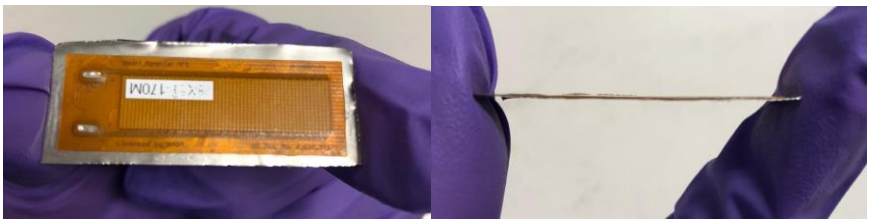

Figure 1.6.1: MFC joined to a carbon steel sheet

The Smart Material company's article *Development of an MFC Bending Element as an Actuator for Sensor Systems* describes three different bending actuator designs [6]. Figure 1.6.2 shows how the monomorph, bimorph and trimorph designs work as an elongation and contraction actuator. The monomorph consists of a substrate attached to the MFC inducing a curve by elongating. In order to perceive a greater deflection, two MFC's should be attached to each other acting as a bimorph actuator. A bimorph will generate a greater expansion between the layers since piezo material on the top expands at the same time piezo material on the bottom contracts. A trimorph involves the addition of a substrate between two piezo materials, however, it reduces the deflection of the actuator but increases the bending motion.

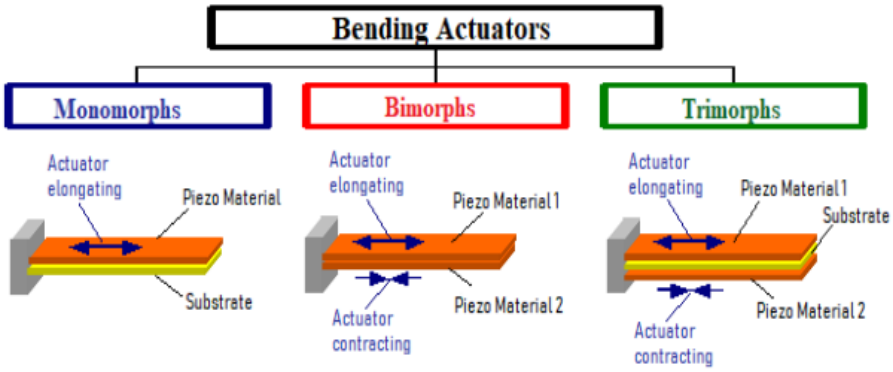

Figure 1.6.2: Design Variants for Piezoelectric retrieved from Smart Material GmbH article

The MFC directed to be a great asset to function as a valve actuator because of its mechanism. However, in order to apply motion to the piezo material a certain voltage must be

applied. The MFC P1 type (d33 effect actuator) operates between -500V to +1500V in order to actuate with a maximum operating temperature of 130℃. This piezo material was not going to accomplish the design requirements of operating in high temperatures from 1000℃ to 1200℃, but its properties were still analyzed. To achieve a greater deflection, the material attached to the macro fiber composite can be steel, aluminum or carbon fiber with a thickness of 0.1 to 0.3 mm.

Most MFCs have been applied in aerospace, civil structures, automotive industry and many others. Most of these applications contain energy harvesting in many different variations that can positively impact the community. MFCs can provide strain actuation, vibration control, and sensing elements. Eduardo Padoin et al studied how to use an MFC to reduce induced structural vibration [36]. The project proposed in this article assured it was possible to improve the behavior of a controlled structure increasing the MFC capability to control the structural vibrations.

Xiao Sun et al designed an MFC for wind turbine blades on fatigue load reduction. This article [37] provides the design and simulation of an MFC to determine a fatigue analysis on a serrated microflap that can reduce the standard deviations of the blade root flapwise bending moment.

1.7 Shape Memory Alloy Theory and Applications

Shape memory alloys (SMA) were discovered by Chang and Read between the 1950s and 1960s [8]. There are many metal alloys, but due to nitinol's properties it is the shape memory alloy that is most commonly known and used. There are various types of shape memory alloys that can be found, such as wire, sheet/plate, and springs. SMAs are smart metals that react to low and high temperatures. An SMA can be deformed at low temperatures from its original profile and will

return to its original shape when exposed to heat. These smart metals experience two phases called martensite and austenite in which occurs at two different temperature ranges [9].

According to the *Shape Memory Polymers: Properties, Synthesis and Applications* article, it states that these phases cause a symmetry change in the crystalline network. As the metal alloy reaches a low temperature and cools down, the martensite phase starts forming by concluding at very low temperatures. The austenite phase starts when heated, so it starts to restructure until it reaches a certain temperature in which the phase has been finished. Figure 1.7.1 visually explains how the metal alloy undergoes these phases.

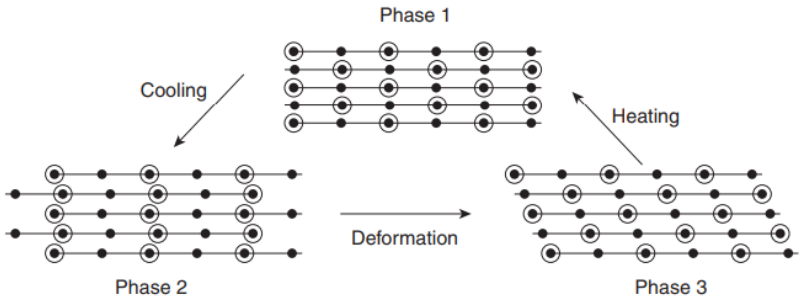

Figure 1.7.1: Shape memory effect retrieved from Shape Memory Polymers: properties, synthesis and applications article

As mentioned before, SMAs are known and commonly used due to its interesting mechanical properties. Nitinol's melting temperature is up to 1310℃, therefore, it can withstand very high temperatures. Using a shape memory nitinol alloy spring as shown in figure 1.7.2 can fulfill the design requirements by being exposed in high temperatures and correctly function as an actuator.

Figure 1.7.2: Nitinol Memory Metal Spring SMA retrieved from Fuxus site

There are many applications of SMAs in aerospace, automobile, civil structures and several others in the industry. SMAs are used in applications for braces and dental arch wires, fixing broken bones using metal plates, bridge structures to dampen vibrations, aircraft and space vehicles because they are lighter and save energy. Hugo Rodrigue et al discuss in their article [38] how SMA wires and springs are implemented as actuators in robots. A model is then developed to discuss the performance and applicability of SMA wires versus SMA spring to be used as actuators. Other articles explain how SMA are used for seismic loads, such as Hui Qian et al investigated a building structure with a super elastic shape memory alloy. The investigations from this article [39] used shaking table tests by experimenting on new super elastic shape memory alloy friction damper. The damper consisted of pre-tensioned super elastic shape memory alloy wires and friction devices. The main function of SMA wires in this research was to provide re-centering capacity, while the integrated friction devices provide the most energy dissipation.

1.8 THESIS OBJECTIVE

The objective of this thesis is to design a high temperature bypass valve for a hybrid system. This will ensure to control the flow exiting from the post-combustor to avoid damaging the fuel cell by blocking the flow and leading it to the turbine. The tasks needed to complete the objective for this thesis are as follow:

Task 1: Design a 3-inch diameter pipe with an expected temperature inlet of 1100˚C to 1200˚C.

Task 2: Investigate and select a composite material to withstand high temperatures.

Task 3: Provide calculations and design blueprints to build prototype.

Task 4: Perform CFD simulations to compare with calculations and experimental work.

Task 5: Describe and explain the design process to complete final design.

1.9 Practical Relevance

The motivation for this project is to design an affordable high temperature bypass valve for a hybrid system. A custom design can be created for any individual searching for a high temperature valve, but it can result expensive. Creating an affordable composite material design would benefit NETL to be used multiple times for any type of experiments. By integrating this valve into the HYPER facility, it would not only limit NETL to perform various experiments, but also would give the opportunity of adding an actual fuel cell to the system. Fuel cells are expensive and can be damaged easily when they are under thermal stress. This valve would help blocking flow exiting from the post-combustor and leading it to the gas turbine. Researchers can control this valve from the control room, not having to control the valve manually and being exposed to high temperatures.

Chapter 2

CALCULATION THEORY

This chapter explains some theory behind the calculations for an MFC and SMA. The calculations shown below can guide the individual to build the prototype. It is important to understand that most of the equations provided in this chapter can be applied when starting to design an SMA spring. However, in chapter 4 three equations provided here helped determine how much force can a spring with specified dimensions provide.

2.1 SHAPE MEMORY ALLOY CALCULATION THEORY

As explained in chapter 1, these smart metals experience two phases called martensite and austenite. The shape memory element has four temperatures that describe the different stages of actuation. Figure 2.1.1 outlines the four temperatures transformation from start to end for austenite and martensite phases. These temperatures and acronyms are as follows: Martensite (1) Finish [Mf], (2) Martensite Start [Ms], (3) Austenite Start [As], and (4) Austenite Finish [Af].

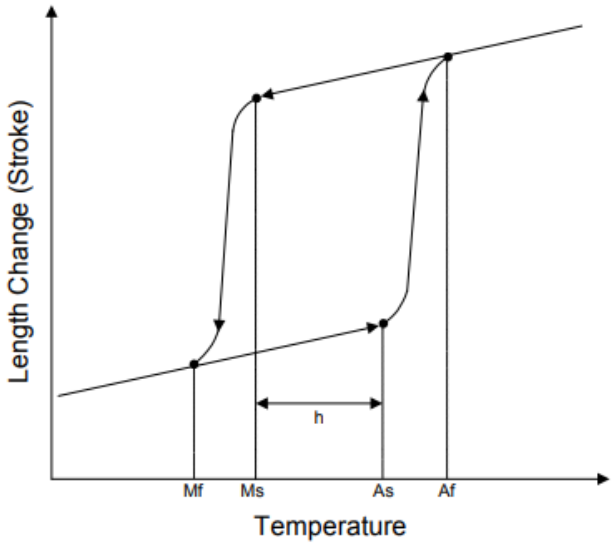

Figure 2.1.1: SMA Length vs Temperature retrieved from *Large Force Shape Memory Alloy Linear Actuator* by Jose R. Santiago Anadon

The shape memory alloy spring offer a great amount of length when force is applied. Waram's [22-24] calculation for shape memory spring procedures are summarized below. Calculations for compression and extension spring are explained further down. Figure 2.1.2 shows a schematic of geometric properties of a spring actuator [29]. The SMA spring design has three geometrical parameters to contemplate:

- Wire diameter
- Average spring diameter
- Number of coils

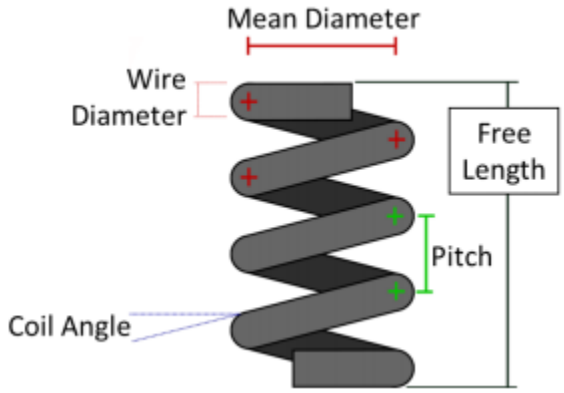

Figure 2.1.2: Spring actuator schematic retrieved from NASA's *Engineering Design Tools for Shape Memory Alloy Actuators: CASMART Collaborative Best Practices and Case Studies*

2.1.1 Compressed Spring Calculations

When a compressed shape memory alloy spring is put under low temperature, the spring compresses and extends when heated as shown in figure 2.1.3. In figure 2.1.3 shown at top is the extended spring described as high temperature length (L_h) and below is the compressed spring described as low temperature length (L_l); length change is defined as stroke (S).

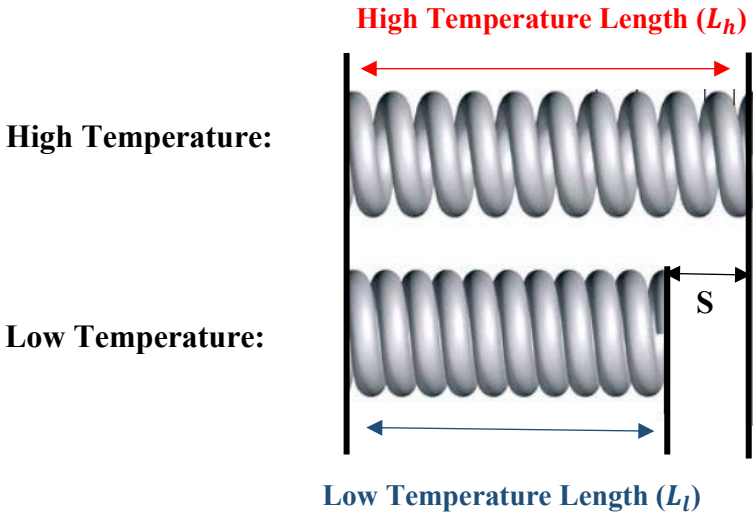

Figure 2.1.3: Example of compression spring reacting to temperature

Two equations are combined to simplify the expression for shear stress in a spring. The first equation in terms of shear stress in a SMA spring was expressed by Liang and Rogers [25] shown below:

$$\tau - \tau_0 = G(\xi)(\gamma - \gamma_0) + \frac{\Theta}{\sqrt{3}}(T - T_0) + \frac{\Omega(\xi)}{\sqrt{3}}(\xi - \xi_0) \quad (1)$$

In which τ, G, γ, Θ, ξ, T, and Ω are shear stress, shear modulus, shear strain, coefficient of thermal expansion, martensite volume fraction, temperature and phase transformation coefficient. The subscript '0' represents the initial conditions. Assuming shear strain is linear in the spring wire cross section, the spring coil diameter is continuous through the spring length. According to Shigley from *Mechanical Engineering Design* textbook [26], shear strain can be related to axial spring deflection through the next expression shown below where d_s, D_s and N are the SMA spring wire diameter, mean diameter of the spring, and the number of spring coils:

$$\gamma = \frac{d_s}{\pi N D_S^2}\delta \quad (2)$$

The expression for shear stress in a spring is finally defined by Aguiar, Liang and Rogers and Shigley [27] as:

$$\tau = \frac{8FD}{\pi d^3} K = \frac{8F}{\pi d^2} CK \qquad \text{[MPa]} \qquad (3)$$

Where F defines the axial load applied, D is the average diameter of the spring, d represents the wire diameter, K is the correction factor applied, and C is known as the spring index as follows:

$$C = \frac{D}{d} \qquad \text{[m]} \qquad (4)$$

The K value in equation (5), also known as Wahl correction factor, is the torsional stress for a solid round bar. This value corrects the shear stress for transverse and torsional shear stresses present in a spring shown below:

$$K_w = \frac{4C-1}{4C-4} + \frac{0.615}{C} \qquad (5)$$

Equation (5) is most recommended for fatigue loading [28] while equation (6) is regularly used for static loading:

$$K_s = 1 + \frac{0.5}{C} \qquad (6)$$

Equation (3) can be used to obtain several wire diameters for acceptable values for the actuator of C between 3 to 12. From equations (3-6) only apply to normal geometry springs which is C>3 and λ<12°. It is also important to note that the maximum shear stress depends on the type of alloy used. An estimated value for 100,000 cycles for Nitinol (Ni-Ti) is 170 MPa. Equation (7) shown below is how to obtain the wire diameters for the actuator:

$$d = \sqrt{\frac{8FCK}{\pi\tau}} \qquad \text{[m]} \qquad (7)$$

Two factors relate to the value of C which are the cycle rate and the envelope volume for the actuator. The cycle rate is a function of the wire diameter, so a value of C can be designated to put up a desired cycle rate. The other method to set the value of C subject to the envelope volume of the actuator which depends on the spring outer diameter and length. The equations discussed next are values that typically come from the company's datasheets. However, the reader will comprehend how to obtain these values to apply to the equations discussed before and after. Equation (8) explains how the average diameter can be obtained from equation (4) by solving for D:

$$D = cd \quad \text{[m]} \quad (8)$$

The inner and outer diameters can also be obtained from equations (9) and (10). The number of turns in the spring is obtained from equation (11). The value of S defines the stroke of the actuator, and the $\Delta\gamma$ is the strain difference at high and low temperatures shown in equation (12):

$$OD = D + d \quad \text{[m]} \quad (9)$$

$$ID = D - d \quad \text{[m]} \quad (10)$$

$$n = \frac{dS}{\pi D^2 \Delta\gamma} = \frac{S}{\pi DC\Delta\gamma} \quad (11)$$

$$\Delta\gamma = \gamma_l - \gamma_h \quad (12)$$

The high temperature shear strain can be obtained from a stress-strain material chart for the assumed high temperature shear stress. Another method is estimating this value assuming a

linear stress-strain behavior, so that the high temperature shear strain can be evaluated from the high temperature stress (τ_h) and shear modulus (G_h) explained below in equation (13). The spring rate for the high and low temperature ranges can also be estimated as shown in equation (14) and (15):

$$\gamma_h = \frac{\tau_h}{G_h} \tag{13}$$

$$k_h = \frac{G_h d^4}{8nD^3} = \frac{G_h d}{8nC^3} \tag{14}$$

$$k_l = \frac{G_l d^4}{8nD^3} = \frac{G_l d}{8nC^3} \tag{15}$$

Once gathering the spring rate, the high temperature deflection can be evaluated through equation (16):

$$\delta_h = \frac{F}{k_h} \quad \text{[m]} \tag{16}$$

To define the low temperature deflection, it is known the stroke is the difference between the low and high temperature spring deflections, so equation (17) can be used to find that value. Equation (18) describes the length of the spring when compressed at low temperatures. At high temperature the spring length is solved through equation (19), and the free length of the spring is defined at equation (20).

$$\delta_l = S + \delta_h \quad \text{[m]} \tag{17}$$

$$L_l = d(n + 3) \quad \text{[m]} \tag{18}$$

$$L_h = L_l + S \qquad [\text{m}] \qquad (19)$$

$$L_f = L_h + \delta_h \qquad [\text{m}] \qquad (20)$$

Since this project proposes a one-way shape memory spring, through equation (21) the required force to revert the shape memory alloy to its original shape can be solved. Equation (22) can calculate the maximum force that can be exerted by the spring:

$$F_r = k_l \delta_l \qquad [\text{N}] \qquad (21)$$

$$F = \frac{\tau \pi d^4}{8ND^3} \qquad [\text{N}] \qquad (22)$$

To evaluate the envelope volume of the spring it can be defined below in equation (23). The envelope volume helps to evaluate the best value for the spring index; however, as discussed before the student can use any of the two different methods.

$$A_e = \frac{\pi OD^2}{4} \qquad [m^2] \qquad (23)$$

2.1.2 Extension Spring Calculations

An SMA extension spring extends at low temperatures and contracts when heated by providing a pulling force. Figure 2.1.4 shows the SMA extension spring actuation below.

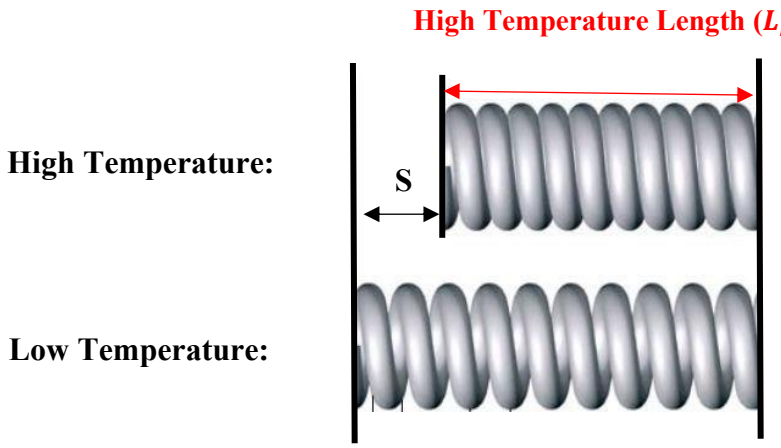

Low Temperature Length (L_l)

Figure 2.1.4: SMA spring extension reacting to temperature

The equations discussed in section 2.1.1 can be used to calculate the number of turns, spring rates, spring diameters, and to reset the spring shape. However, the spring lengths are different from the compressed spring to the extended spring because the extended spring is reversed from the compression lengths so they must be reassessed. Equation (24) evaluates the spring body length in a fully compressed spring where n is the number of turns of the spring. The length at which the spring shape setting takes place can be defined as a function of the body length in equation (25). When the spring is under high temperatures the length can be obtained from equation (26). Finally, equation (27) is used to calculate the low temperature length.

$$L_b = d(n+1) \quad \text{[m]} \quad (24)$$

$$L_f = L_b + 2(ID) \quad \text{[m]} \quad (25)$$

$$L_h = L_f + \delta_h \quad \text{[m]} \quad (26)$$

$$L_l = L_h + S \quad \text{[m]} \quad (27)$$

2.1.3 Shape Memory Alloy Activation

Shape memory alloys can be heated and activated by passing direct current through them or heating them up. Their length and cross-sectional area can be used to calculate the resistance shown in equation (28). In which ρ represents the SMA resistivity, A its cross-sectional area, and

L is the free length of the alloy. Through Ohm's Law the voltage required can be calculated from equation (29), and the power requirement on equation (30).

$$R = \frac{\rho L}{A} \qquad [\Omega] \qquad (28)$$

$$V = IR \qquad [V] \qquad (29)$$

$$W = IV = I^2R \qquad [W] \qquad (30)$$

Waram explains a detailed method in his textbook to estimate the current value and cooling times for the actuator [30]. He derived those formulas by testing a specific type of alloy under motionless and forced air conditions. The thermo-mechanical properties of shape memory alloys differ critically from alloy to alloy, so it is mostly recommended to define the activation current through testing.

2.2 MACRO FIBER COMPOSITE CALCULATION THEORY

A piezo actuator has two features which are the idle stroke and the blocking force. The blocking force is the maximum force generated by the actuator. This force is defined when the displacement of the actuator is entirely blocked, so it works against a load with an infinitely high stiffness. In order to estimate the stiffness, the blocking force is measured when the actuator is displaced and then reverted to the initial position with an external force (blocking force). The idle stroke is a small gap between the piezoelectric actuator and the wall of the pipe.

Equation (31) is used to calculate the required deflection from the cantilever where $u, L \; and \; R_K$ are defined as free deflection, actuator length and curvature of the structure. In order to solve for R_K, equations (32-35) were combined assuming the curvature of the actuator, the strain

from figure 2.2.1 [6], the longitudinal forces defined by N, so equation(35) defines the curvature of the structure combined with all equations mentioned:

$$u = \frac{1}{R_K} * \frac{L^2}{2} \tag{31}$$

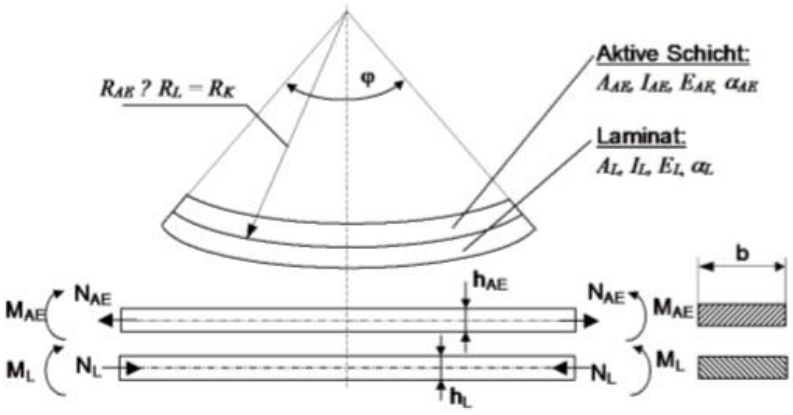

Figure 2.2.1: Bending actuator schematic retrieved from *Development of an MFC Bending Element as an Actuator for Sensor Systems*

$$k = \frac{1}{R_K} = \frac{M_{AE}}{I_{AE} * E_{AE}} = \frac{M_L}{I_L * E_L} \tag{32}$$

$$\alpha_{AE} * T + \frac{N}{E_{AE} * A_{AE}} + \frac{h_{AE}}{2} * \frac{1}{R_K} = \alpha_L * T - \frac{N}{E_L * A_L} - \frac{h_L}{2} * \frac{1}{R_K} \tag{33}$$

$$N_{AE} = N_L = N, so\ N * \frac{h_{AE} + h_L}{2} = M_{AE} + M_L = M \tag{34}$$

$$\frac{1}{R_K} = (\alpha_L - \alpha_{AE}) * T * [\frac{2}{h_{AE} + h_L} * \frac{I_{AE}}{A_{AE}} * \left(1 + \frac{I_L E_L}{I_{AE} E_{AE}}\right) * \left(1 + \frac{A_{AE} E_{AE}}{A_L E_L}\right) + \frac{h_{AE} + h_L}{2}]^{-1} \tag{35}$$

$$\frac{1}{R_K} = k = \varepsilon_{MFC} * [\frac{2}{h_{AE} + h_L} * \frac{I_{AE}}{A_{AE}} * \left(1 + \frac{I_L E_L}{I_{AE} E_{AE}}\right) * \left(1 + \frac{A_{AE} E_{AE}}{A_L E_L}\right) + \frac{h_{AE} + h_L}{2}]^{-1} \tag{36}$$

Now equation (37) can be used to find the force needed to push the cantilever tip shown below:

$$F_{block} = 3 * \frac{u*EI}{L^3} \tag{37}$$

Equation (38) estimates the dynamic behavior of the piezoelectric, where $a_{accel}, m_{structure}, F_{block}$ represent acceleration, mass structure and block force.

$$F_{block} = m_{structure} * a_{accel.} \tag{38}$$

Most of the equations discussed in this chapter were obtained from *Development of an MFC Bending Element as an Actuator for Sensor Systems*, so in order to compare results it would be best to test the actuator and compare calculations with a force vs displacement graph.

Chapter 3

DESIGN MODEL

This chapter explains how the design of the valve has been changing as most materials have been analyzed. The final design will briefly explain the movement of the actuator and how this will achieve the design requirements. It also includes a list of supplies to build a testing prototype of the valve and a final prototype to integrate it in the hybrid system.

3.1 DESIGN CONSTRAINTS

Many aspects of any design project must be considered to determine the feasibility of a product. The success of a project depends mainly on the scope, time, budget, and quality. Sustainability and manufacturability go under quality referring to the ability of designing a product to perform under normal operating conditions for a given amount of time. While choosing an actuator that was reliable, the budget also had to be considered. Both the MFC and SMA offered great abilities for the valve, however, the MFC was more expensive. SMA are cost-effective and their mechanical properties met the standards for the project.

Time is accountable when testing, in which the MFC took most of the project's schedule while confirming its functionality. Ordering materials, building prototypes, investigating more about the project, and testing the prototype are important tasks to work alongside a schedule. Budget is an important factor when developing a high-quality project. Selecting parts, making modifications, manufacturing lifetime product were considered by choosing the broadest parts to ensure a durable artifact. The focus in this project is to design a high-performance valve to accomplish most proposals from laboratories.

3.2 BOUNDARY CONDITIONS

Air is considered in the computational model discussed in chapter 4, and at the lab during testing. The flow rate delivered for a lab prototype and final product for the HYPER facility is different. The prototype should deliver flow near to 0-5 g/s through the pipe, in which a mass flow meter will verify this value. As for the actual final product it must deliver near to 50-100 g/s, and this could be verified by sending the final design to the HYPER facility to test it. The lab prototype temperature inlet must be 100℃ with the help of a heater or heat exchanger. The boundary conditions detailed in tables 3.1 and 3.2 were used to design and to be tested in the prototype.

Table 3.1: Lab Prototype Boundary Conditions

Inlet Boundary Conditions	
Mass Flow Rate	0-5 g/s
Temperature	100℃
Actuator Electric Activation	6-12 V
Pipe Material (Wall)	PVC

Table 3.2: Final Product Boundary Conditions

Inlet Boundary Conditions	
Mass Flow Rate	50-100 g/s
Temperature	1100-1200 ℃
Actuator Electric Activation	6-12 V
Pipe Material (Wall)	Steel

3.3 APPROACHING THE DESIGN

As explained earlier the first important task was designing the valve. This was accomplished by using the Bernoulli equation and calculating the pressure drop, friction factor,

length of the pipe, internal diameter of the pipe, average velocity, fluid density and the gravitational constant. Many assumptions were considered to accomplish the goal of the design, which helped to shape the path of the design. After visualizing the idea of the design, the second important task was finding the material for the actuator.

As stated above, the Bernoulli equation along with other equations shown below were used to calculate many values. Starting a design is difficult at first because is hard to know where to start. Many assumptions were made while brainstorming for a design, but also applying equations from fluid mechanics to estimate outcomes. Shown below is a one of the starting process for this project. The dimensions used for these calculations were of a 3-inch pipe diameter assuming steel roughness. The purpose was to get an idea of the velocity this valve was going to confront, but at the end for sure the velocity was too high. Another important task was calculating the pressure drop for an elbow and a sweep tee design.

$$Re = \frac{4\dot{m}}{\pi D\mu} = \frac{4(0.1\frac{kg}{s})}{\pi(0.0779\ m)(520.9*10^{-7}\frac{N*s}{m^2}} = 31{,}379.2 \quad \boldsymbol{TURBULENT} \tag{39}$$

$$Friction\ Factor = \frac{e}{D} = \frac{4.5*10^{-5}\ m}{7.79*10^{-2}\ m} = 5.78 * 10^{-4} = \sim 0.045 \tag{40}$$

$$V_{avg} = \frac{4\forall}{\pi D^2} = \frac{4(3.93*10^{-1}\frac{m^3}{s})}{\pi(7.79*10^{-2})^2\ m^2} = 82.6\frac{m}{s} \tag{41}$$

$$h_L = h_{L,maj} + h_{L,min} = f\frac{L}{D}\frac{V^2}{2g} + \Sigma k\frac{V^2}{2g} \tag{42}$$

$$h_{L,maj} = (0.046)\left(\frac{0.254\ m}{0.078\ m}\right) * \frac{\left(83\frac{m}{s}\right)^2}{2\left(9.81\frac{m}{s^2}\right)} = 52.6 \tag{43}$$

$$h_{L,min} = \Sigma k \frac{V^2}{2g} = (5.78\ m)(\frac{\left(83\frac{m}{s}\right)^2}{2\left(9.81\frac{m}{s^2}\right)} = 2028.08 \quad (44)$$

$$h_L = 52.66 + 2028.08 = 2080.7 \quad (42)$$

$$\Delta P = \left(2.54 * 10^{-1}\frac{kg}{m^3}\right)\left(9.81\frac{m}{s^2}\right)(2080.7) = 5183\ Pa = 0.05\ bar \quad (45)$$

High temperature materials were studied on their mechanical properties by investigating how flexible they can operate. In this design, the actuator, the hinges, and the plate are the special features that were integrated to accomplish the goal of the project. The following sections thoroughly articulate how the valve must work under assigned boundary conditions.

3.4 Preliminary Designs

Various designs were proposed for the high temperature valve by adding piezoelectric actuators. Brainstorming was important to put designs together and understand how the valve can deliver a great work performance. The goal of design #1 on figure 3.2.1 was to puncture holes around the pipe and use piezoelectrics resting inside over each hole to block the flow from exiting the pipe. However, whenever voltage was subjected to the piezoelectric, it would cause the actuator to vibrate and the flow would escape. At last the design was not the best option to use for the project.

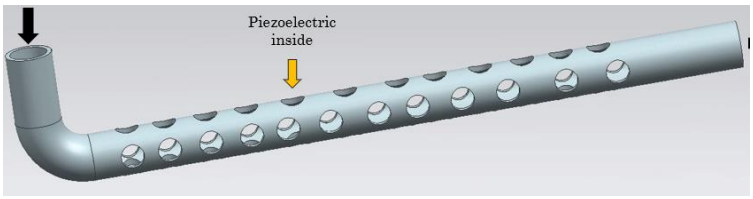

Figure 3.2.1: Design #1

Design #2 proposed to use rectangular piezoelectrics inside the pipe, so that when voltage was applied to each actuator it would make it bend upward by preventing flow to pass through the pipe. There were many factors to contemplate for this design by having a turbulent flow or high pressure drop.

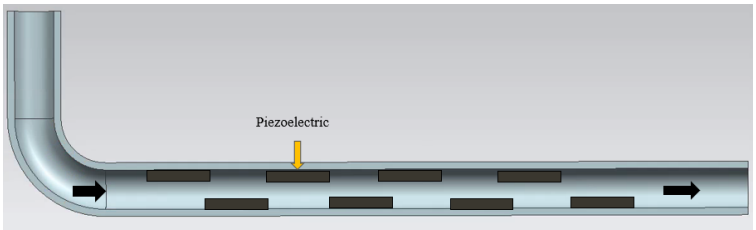

Figure 3.2.2: Design #2

A Y-shape pipe was proposed for design #3 alike #4 by directing controlled flow to the fuel cell and turbine. The pipe would have a circle wall inside punctured with holes and each of the holes having an actuator on top. This design offered the same goal as design #1 but having "more controlled" flow.

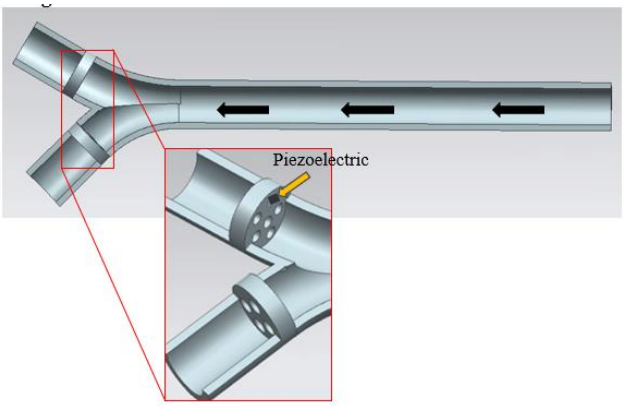

Figure 3.2.3: Design #3

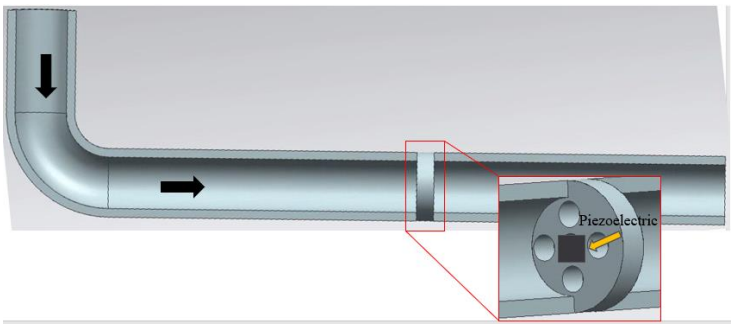

Figure 3.2.4: Design #4

In the end these designs were not chosen because of high pressure losses, difficult to manufacture, and most of the ideas lead to failure while trying to implement the movement of the actuator.

3.5 VALVE DESIGN

After investigating the material for the valve, two designs were proposed to utilize three different actuators. The first design shown in figure 3.5.1 has a sweep tee shape in an angle of 45˚. Design #1 was planned to use the lithium niobate piezoelectric or the MFC for the actuator in case one or the other failed. This design utilizes a 3-inch diameter pipe with an expected temperature inlet of 1100˚C - 1200˚C, and a 4-bar pressure with an expected valve mass flow rate of 50 – 100 g/s. This specific shape along with the angle was selected to have a controlled smooth flow passing through the pipe to avoid pressure drop. The design requirements are listed more in detail below in table 3.3.

Table 3.3 Valve Design Requirements

Design Requirements	
Dimensional Length Scale (in)	3’’

Temperature Inlet (℃)	1100 - 1200
Pressure (bar)	4
Valve Mass Flow Rate Expected (g/s)	50-100

This bypass pipe has a special feature, which is a square pipe shape located at the center approximately 6-inches long. The purpose as to why this shape was utilized in the design is because the MFC and the Lithium Niobate piezoelectric working as an actuator inside the pipe is a rectangular shape. Leading the fluid from a circular shape to a rectangular shape of the pipe serves as a great advantage in the design to at least expect a uniform flow passing through the pipe. Many articles have studied the behavior of a square cylinder [19] which has interesting topic of discussion, analyzing corners of the square that can deliver many different behavioral data when exposed to an airflow. Otherwise, if complications arise with the airflow, then a honeycomb airflow straightener can also be used in the setup.

After the square shape, the pipe will return to its standard circular shape. The distance from the square shape to the circular shape is highly important to have a smooth airflow. Figure 3.5.1 shows two piezo plates fixed at one end from the wall of the pipes. These two piezo plates will be attached from a custom piezoelectric mount design, which will have two small holes on the top to connect two cables to a power supply and control the motion of the piezoelectric.

These piezoelectrics are applied a specific voltage at a fixed end to cause a movement to partly open and let the airflow pass through. When no voltage is supplied to the piezoelectric, it will block the airflow by remaining closed. Whenever the voltage is applied to the piezoelectric, it should bend up or down, working as a gate by opening and closing. Piezoelectrics are utilized everywhere and can function as an actuator or a sensor, but in this case, it is being used as an

actuator. As stated before, the piezoelectric or MFC are the actuators acting as a valve, thus working as a gate in design #1.

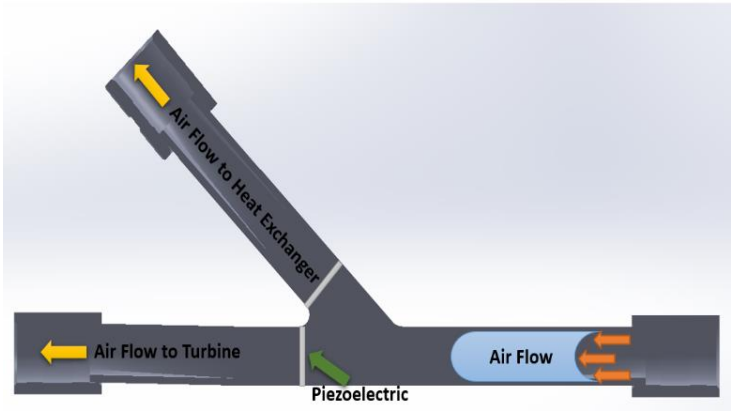

Figure 3.5.1: Design #1 for MFC and lithium niobate piezoelectric

Design #1 discussed before seemed achievable, but to have a more efficient assembly it was better to work with design #2. Figure 3.5.2 shows design #2 with SMA springs and nitinol plates put together. The design will contain a total of six SMA springs, in which the nitinol plate will have the six SMA springs attached. The plate along with the springs are attached from a hinge and the hinge will be glued to the pipe. In order to accomplish the work of the gate, a hinge is very flexible to move the actuator up and down.

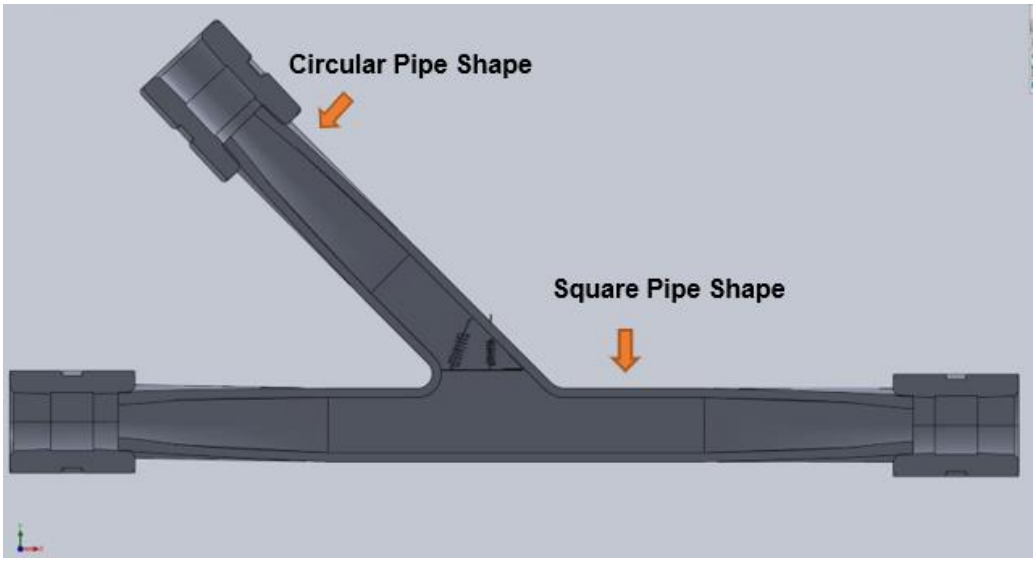

Figure 3.5.2: Design #2 using SMA spring and nitinol plate

The use of a custom piezo mount design in design #1 was mentioned, but this mount was not going to help achieve a complete bending motion to the MFC and piezoelectric. If the actuators do not have a bending support, then the results would be catastrophic because the actuators would not last long and could break. This is the reasoning of why a hinge is convenient to use. The hinge will be manufactured out of silicon carbide material. Silicon carbide is listed in the top ten metals to withstand very high temperatures with a melting point of 2820℃ [17].

Table 3.4 Design #2 Materials

Materials	
A	1/2'' Spring (3 total)
B	1'' Spring (3 total)
C	Nitinol Plate
D	Hinge

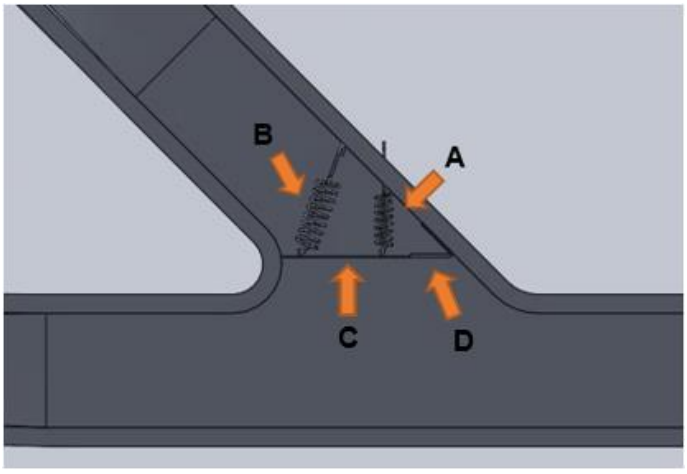

Figure 3.5.3: Design #2

The reason as to why a total of six springs must be used is because one SMA spring provides up to 4 Newtons (N) (408 g) of force upon contraction or expansion. The nitinol plate is going to have three $\frac{1}{2}$-inch spring at the bottom (**A**) and three 1-inch spring at the top (**B**) to help expand and block the air flow as shown in figure 3.5.3. When the nitinol plate is exposed to heat, it will always maintain a straight form to avoid any bending. The six springs are going to be insulated in order to control the motion whenever the researcher decides to open the actuator since the heat of the air flow inside the pipe will keep spring expanding.

To conclude, design #2 will be built using one plate with six 0.3-inches long wires shaped in semicircle and soldered to the plate. This way the springs are going to grasp from the plate and the pipe will have six holes to insert one end of the springs. The wire at the end of each spring will be taken out through the six holes to control its motion by applying current with a power supply. The plate is going to be attached on the hinge and the hinge from the pipe with the use of ceramic adhesive that can resist over 2000℃, or through welding [18].

Table 3.5 shows a list of materials needed to build the final design of the valve:

Table 3.5 List of materials for final design

Item #	Description	Quantity
1	SCH 40 Pipe	1
2	SMA Spring	6
3	SMA Plate 8'' x 12''	1
4	Silicon Carbide Plate 8'' x 12''	1
5	SMA Wire (connects plates to spring) 1-ft	1

6	Soldering Iron	1
7	Power Supply (control SMA springs)	1
8	Ceramic Adhesive (2000℃)	1

3.6 FUTURE WORK SETUP

A prototype is going to be built and tested to gather data on how much deflection the SMA spring attached to the plate will experience when in motion. Figure 3.6.1 demonstrates the prototype setup to test the actuator's performance under pressure, heat and voltage. In order to validate the function of the actuator, two SMA springs attached to a nitinol plate are planned to be used to be tested due to its great mechanical properties of deflection and resistance in high temperatures.

The prototype design is different from the actual in order to mainly focus in the behavior of the airflow and the deflection of the springs. A list of materials is listed below shown in table 3.6. An air source is going to be connected through item **D** and the flow meter in item **A** will read the flow rate passing through. Item **C** is shown in figure 3.6.2 of how the actuator is going to be fixed inside the PVC pipe with a close-up showing how the plate and springs are attached as shown below.

Table 3.6: List of Materials for Test Prototype

Materials	
A	Flow Meter
B	$2\frac{1}{2}$'' PVC Pipe

C	Actuator Mount
D	Air Source Connector
E	Valve
F	Power Supply
G	Soldering Iron
H	SMA Spring (2)
I	Nitinol Plate

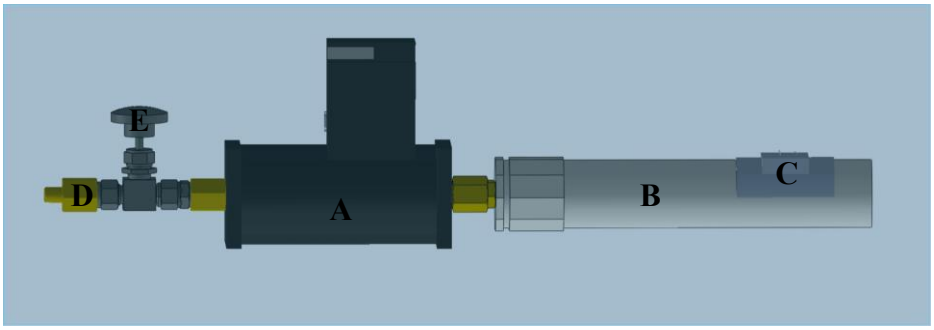

Figure 3.6.1: Valve prototype design

Applying different voltage inputs to the SMA spring using a power source will help find a relationship between the flow rate going through the pipe. The actuator is planned to be exposed to different temperatures at the same time voltage is supplied to analyze its behavior under these conditions. The power supply will flow current to the top of the wires to control the actuator's mechanism. In order to test the prototype, there will be a flow source (fan or gas cylinder) connected to the end of the $2\frac{1}{2}$-inch pipe and deliver near 0 to 5 g/s through the pipe and valve. At different points of the pipe, the flow rate passing through the pipe is going to be measured using a mass flowmeter. The goal of this experiment is to achieve a mass flow rate of 5 g/s. This prototype will mainly help validate the function of the actuator's deflection.

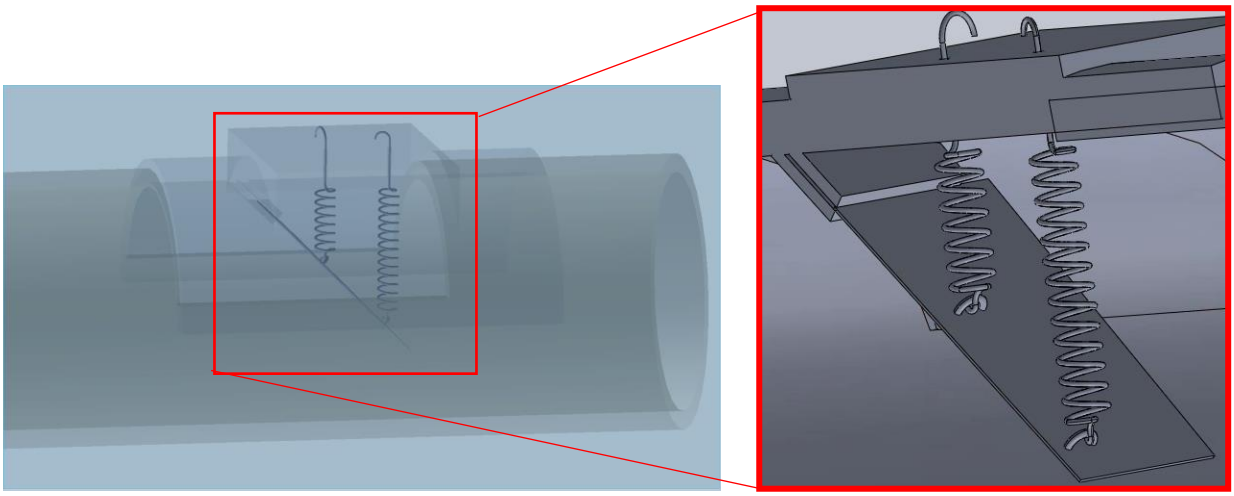

Figure 3.6.2: Actuator inside of prototype

3.7 Safety Analysis

During the design phase it is important that each component integrated is subject to a safety analysis. Shown below are flow diagrams that mention precautions from the design and afterwards an explanation of safety measures.

Table 3.7 Safety analysis

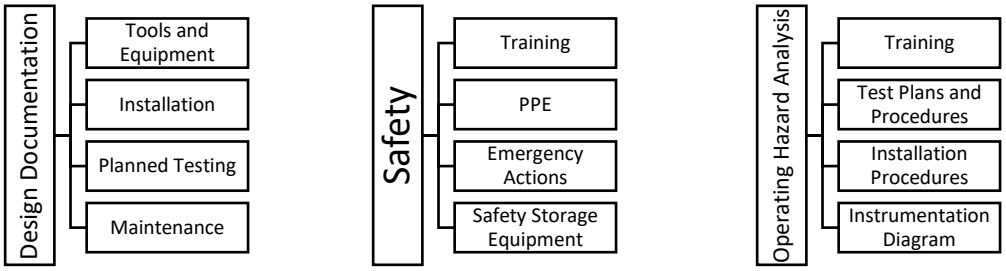

A design documentation must be provided to all team members to understand the project and tasks that must be delivered. The design documentation must contain tools and equipment used while building the prototype of the design and the final design integrated to the system. It should also include installation describing where each part is located correctly to avoid any tragedies before it is operated. Any type of testing should be discussed and analyzed before to

understand what data is needed and how it should be operated. Maintenance should always be provided to any type of machine to avoid any errors while testing or electrical failures.

For any type of operations there should be safety measures provided for the operators. Before any operation there should be training provided for the workers to understand safety precautions. Safety equipment storage should also be checked regularly to have everything in stock. All safety equipment should be provided to the operator and the operator is responsible to wear it. One type of training is the Personal Protective Equipment (PPE) that explains the type of equipment that protects the operator against health or safety risks at the lab.

PPE is important because it provides instructions, procedures and training that encourage the person to work safely. The following are some types of PPE provided by the Health and Safety Executive that can be used [20]:

Table 3.8 Types of PPE

Eyes	Head	Ears	Hands	Feet
•Goggles •Face Screens •Face Shields •Visors	•Safety Helmets •Hairnets	•Earplugs •Earmuffs	•Gloves	•Safety boots •Shoes with protective toecaps

While operating any type of machine, training must be provided to understand how to run the machine properly. All test plans and procedures should be revised earlier with the supervisor to check any errors and confirm to run the experiment. An instrumentation diagram should also be provided to every team member to know where all parts are in the machine. The instrumentation diagram will help the person to study the machine correctly and understand how it operates properly.

Safety analysis is highly important in any work area to avoid accidents. All safety measures should be responsibly taken with seriousness to achieve the task correctly and safely.

However, if no safety measures are provided to a team member then approach the supervisor to receive them immediately.

Chapter 4

RESULTS AND DISCUSSION

This chapter clarifies how ANSYS was used to perform simulations on the final design. It explains how the design reacts under laminar flow. Through the analysis of these simulations, it assures the efficiency of the design to build a prototype and compare results. A prototype and a test procedure are planned once the design of the valve is concluded. Spring calculations included in this chapter explaining how much force each spring provides and the drag force of the air flow.

4.1 SPRING DESIGN CALCULATION

The valve was designed with six extension springs, where the spring extends when heated as mentioned before. Using equations from chapter 2 can calculate the force one spring can provide. The force sometimes has a major or minimal change depending on the wire diameter, outer diameter, and the number of coils as explained in chapter 2. The wire diameter and spring diameter from the spring in the design are 0.75 mm (wire diameter) and 6.5 mm to 9 mm (spring diameters). Three equations from chapter 2 are shown below along with the calculation of the force.

$$C = \frac{D}{d} = \frac{6.5\ mm}{0.75\ mm} = \frac{0.0065m}{0.00075\ m} = 8.67\ m \quad (4)$$

$$K_w = \frac{4*C-1}{4*C-4} + \frac{0.615}{C} = 1.17 \quad (5)$$

$$\tau = \frac{8*F}{\pi*d^2} * (C * K) \rightarrow 170\ MPa = \frac{8*F}{\pi*(0.00075\ m)^2} * (8.67m * 1.17) = 4\ N \quad (3)$$

For many applications the maximum safe stress for the wire is 170 MPa, so this shear stress was considered in these calculations. One spring with the specified dimensions delivers 4 N, so

the spring consisting at least 20 coils can be stable. The number of coils help the force exerted by the spring to stay in firm position. This is the reason why six springs are part of the valve design to accomplish the goal of the actuator. Table 4.1 gives estimates as to how much current and force to expect from a Flexinol® actuator spring. Once calculating the force of the spring, this table was reasonable to use to calculate the current and voltage needed to activate the actuator.

Table 4.1: Guidelines for actuator spring retrieved from Flexinol®

Spring Wire Diameter (mm)	Resistance (ohms/meter)	Heating Pull Force (g)	Approximate Current (A)
3.45	4.33	243	3.4
2.54	8.27	139	1.9
1.37	29.13	39	0.7

Now using the Ohm's Law, the voltage required for activation can be calculated as follows:

$$V = I * R \tag{29}$$

However, typically these actuators require voltage around 6-12 V. Table 4.1 can be used for assumptions, but it is also important to test the actuator with safety precautions.

4.2 Laminar Flow Analysis on Test Prototype Design

An analytical solution was conducted to find the drag force of the flow passing through the pipe as shown below:

$$F_{D=\frac{1}{2}\rho U^2 C_d A} \tag{46}$$

$$F_D = \frac{1}{2} * \left(1.28 \frac{kg}{m^3}\right) * \left(30 \frac{m}{s}\right)^2 * (1.15) * (0.036\, m^2) = 24\, N$$

Table 4.2: Drag force equation variables

Symbol	Definition
$\boldsymbol{F_D}$	Drag force generated by the body (N)

ρ	Density of the fluid ($\frac{kg}{m^3}$)
U	Speed of the body or the fluid ($\frac{m}{s}$)
$\boldsymbol{C_D}$	Experimentally determined drag force coefficient
A	Surface area of the body perpendicular to the flow (m^2)

According to this result it is expected the drag force of the flow against the plate to be 24 N. As stated previously in section 4.1, one spring provides 4 N of force thus six springs were added to the design providing 24 N of force.

The CFD from the test prototype was used to analyze the flow to compare the drag force with analytical results. The velocity inlet input in figure 4.2.2 was 30 m/s in order to compare the results to the analytical solution. It is understandable minor leakage will exist, but the plate will block as much flow as possible. A medium mesh size was held for this CFD because the fine mesh size was failing for results. The drag force determined with the CFD on figure 4.2.4 and 4.2.5 method was of 24 N similar to the calculations discussed previously.

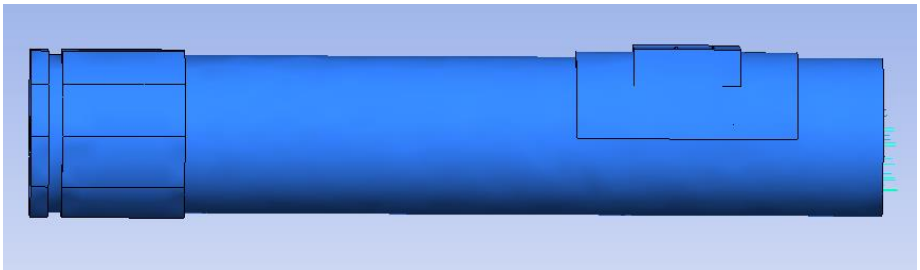

Figure 4.2.1: Outside of pipe in ANSYS

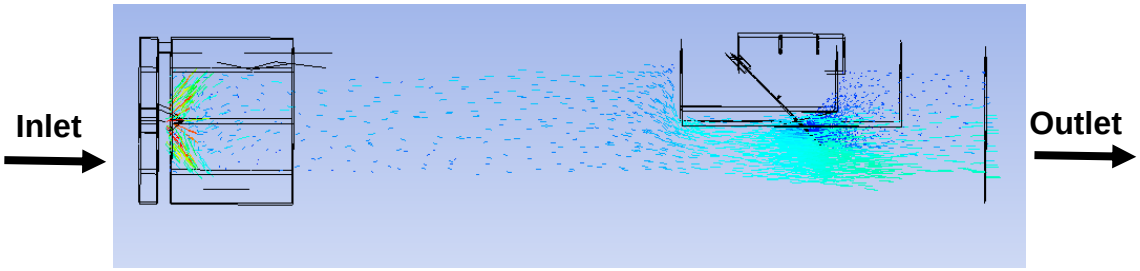

Figure 4.2.2: Fluid streamlines inside the pipe

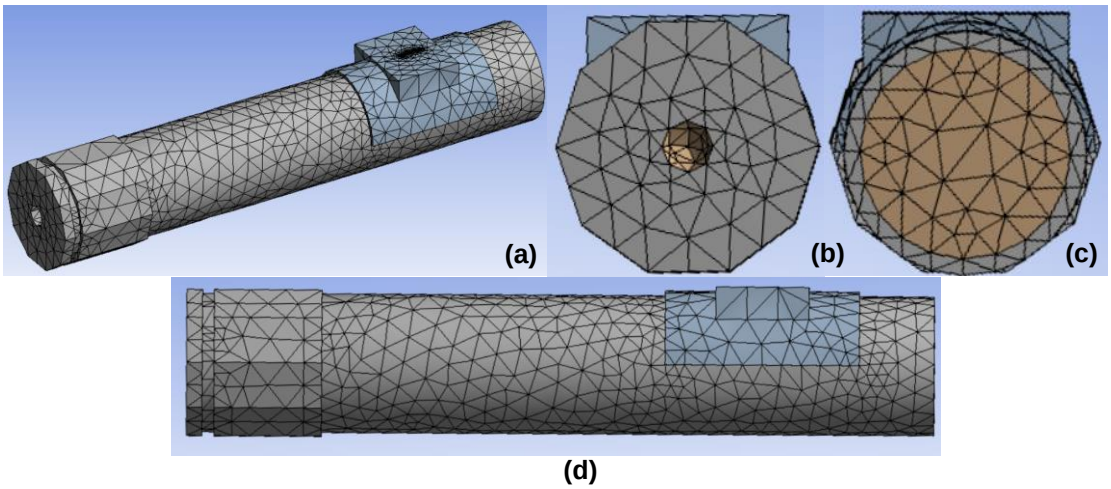

Figure 4.2.3: (a) Isometric View (b) Front View (c) Back View (d) Side View

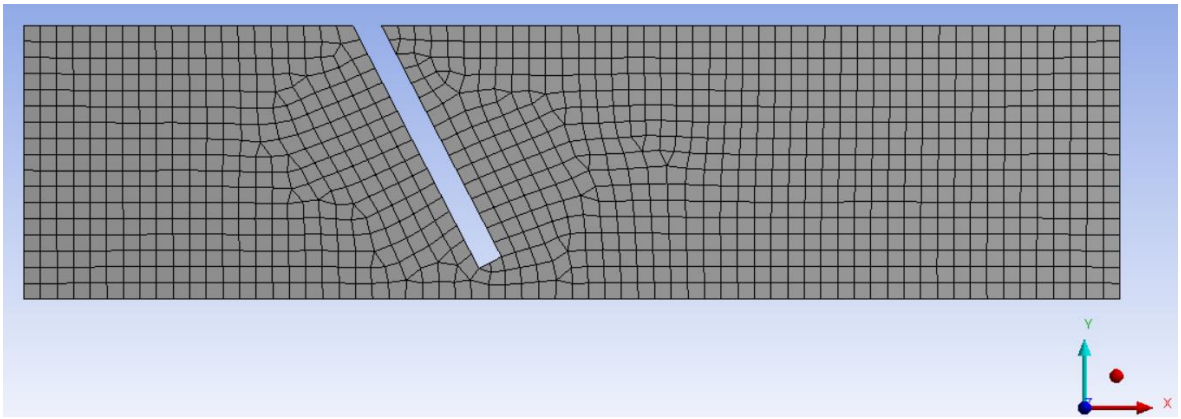

Figure 4.2.4: 2D Valve Mesh Design

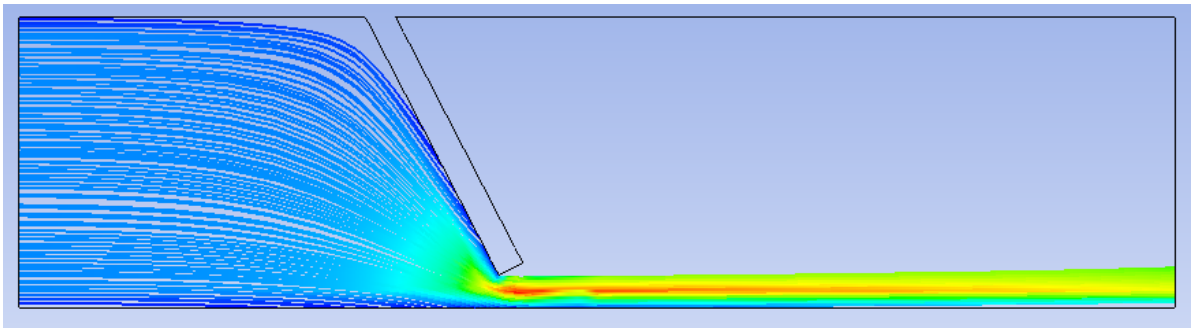

force	(n)
pipe_wall	-24.186148

Figure 4.2.5: 2D Valve Design Velocity Vector and Drag Force Result

The following tables 4.3 and 4.4 explain the procedures along with boundary conditions that were used for the CFD.

Table 4.3: Ansys Model Boundary Conditions for Laminar Flow

Tab	Settings	Value
Geometry	Dimensions	Diameter: 2.5 inches Long: 6 inches
Mesh	Sizing > Turn off *Proximity and Curvature*	*Uniform* or *Adaptive*
	Create Named Selections	Inlet (1) Outlet (2) Pipe (Body) Fluid (Air)
Setup	Options > Double Precision	
	Processing Options > Serial	
	Models > Viscous	Laminar
	Materials > Fluid and Solid	Air and Aluminum
	Cell Zone Conditions > Fluid and Pipe	Air and Aluminum (Verify)
	Boundary Conditions > Zone > Inlet > Velocity Magnitude	30 m/s
Solution	Monitors > Residuals > Continuity, x-velocity, y-velocity, z-velocity	1e-7 (accuracy)
	Solution Initialization > Initialization Methods > Standard Initialization > Compute from	All zones > Initialize
	Run Calculation > Number of Iterations	1000 (Maximum Iterations for accuracy) > Calculate

Results	Velocity Vector > Domains > Fluid > Locations	Fluid
	Analyze velocity vector, contour, velocity streamlines*	

Table 4.4: Ansys Model Boundary Conditions to Find Drag Coefficient and Drag Force

Tab	Settings	Value
Geometry	Dimensions	Diameter: 2.5 inches Long: 6 inches
Mesh	Sizing > Turn off *Proximity and Curvature*	*Uniform* or *Adaptive*
	Create Named Selections	Inlet (1) Outlet (2) Pipe (Body) Fluid (Air)
Setup	Options > Double Precision	
	Viscous > k-epsilon	
	Materials > Fluid and Solid	Air and Aluminum
	Cell Zone Conditions > Fluid and Solid	Air and Aluminum
	Boundary Conditions > Inlet > Velocity Magnitude, Mass Flow Rate	30 m/s, 0.05 kg/s
	Boundary Conditions > wall-plate > Wall Motion > Stationary Wall > Shear Condition > No Slip > Toughness Models > Standard	
Solution	Report Definitions > New > Drag Coefficient > Force Vector > 0,0,1 > wall-plate	
	Report Definitions > New > Lift > Force Vector > 0,1,0 > wall-plate	
	Report Definitions > New > Force > Force Vector > After computing drag force can be solved in any vector	
	Monitors > Residual > Continuity, x-velocity, y-velocity, z-velocity	1e-7
	Initialization > Hybrid Initialization > Initialize	
	Run Calculation > Maximum Iterations > 1000 > Calculate	
Results	Go back to Report Definitions and compute for Drag Coefficient and Drag Force	

4.3 Laminar Flow Analysis on Valve Design

A final analysis was made to the Y-shape pipe design to analyze the reaction of the air flow inside. The velocity applied to this simulation was of 30 m/s in order to compare and verify with

the results on section 4.3. The drag force can also be obtained with equation 46 by using different velocities and changing the area as shown below.

Table 4.5: Y-Shape Model Boundary Conditions

Velocity	30 m/s
Dimensions	Diameter: 3 inches Long: 6 inches

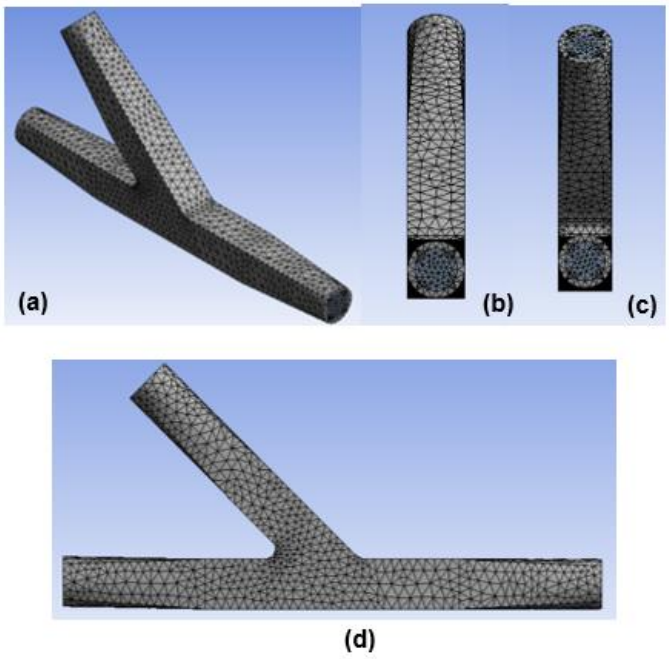

Figure 4.3.1: Mesh for Y-shape Model (a) Isometric View (b) Front View (c) Back View (d) Side View

$$F_D = \frac{1}{2} * \left(1.28 \frac{kg}{m^3}\right) * \left(30 \frac{m}{s}\right)^2 * (1.15) * (0.0456\ m^2) = 30\ N$$

Procedures shown in tables 4.3 and 4.4 were also performed to analyze the Y-shape model, but with different dimensions and other boundary conditions stated in the chart. The drag force expected analytically for the Y-shape model is of 30 N assuring the design only needs the addition of two more springs to achieve blockage with a total of 8 springs. The drag force also determined from the CFD method was of 24 N. The reason for the big difference can be found in the size of

the generated mesh and the number of iterations. Computational results must be compared with experimental results to understand the dynamics of the design better.

The recorded data was put together in a graph to compare the calculated drag force and the drag force from ANSYS Fluent. Figure 4.3.2 shows the change of drag force as a function of velocity attaining manual and CFD calculation results.

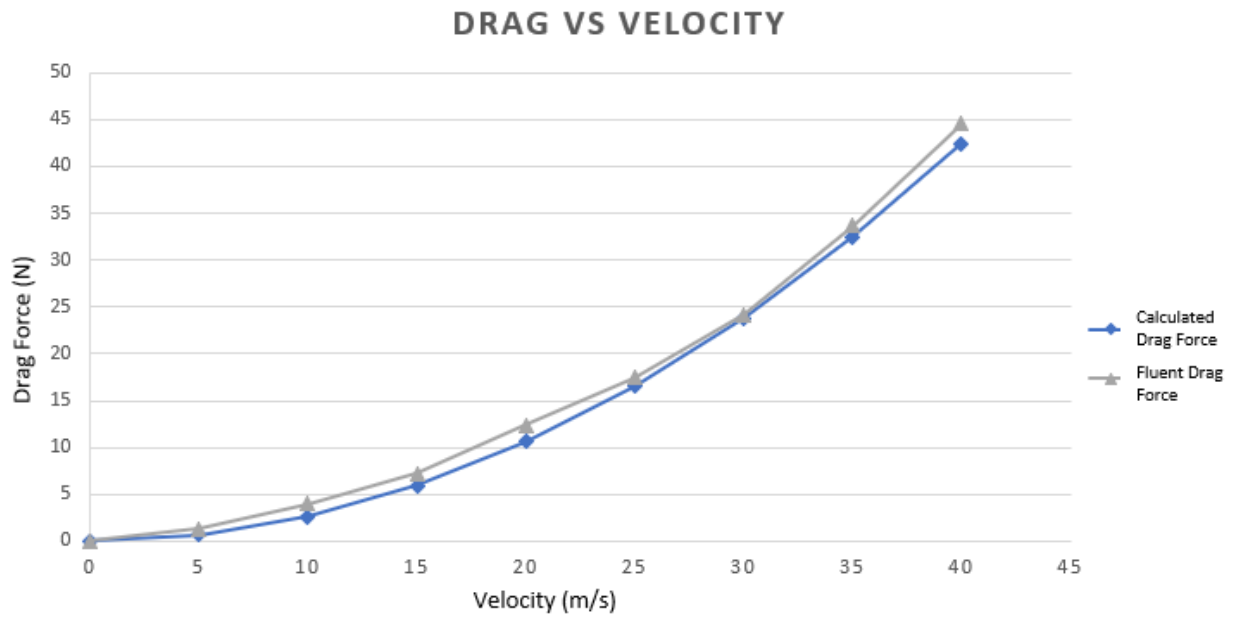

Figure 4.3.2: Drag Force vs Velocity Graph

Through the analysis and results from chapter 4, it provides the researcher with many assumptions and ideas on how to start building the design provided or improving it and creating a new one. The expectation of this research project is to start developing new ideas for high temperature valve usage, especially under the environment of this research project working with a SOFC/GT hybrid system.

Chapter 5

CONCLUSION

This study proposes a high temperature and pressure bypass valve to control the airflow going towards a turbine and heat exchanger during the startup of a SOFC/GT system. To control the high temperatures exhausted from the post-combustor, a bypass valve will be placed before the heat exchanger to regulate the airflow going to the fuel cell and avoid thermal stress on the material. The following are key points this study determined:

1. An SMA spring provides 4 N of force, whereas an MFC generates about 4kN/cm^2 of force for the active cross section of the MFC.
2. Two different setups are to be developed. One of the setups is a room temperature setup that can withstand 100°C, and the other is a high temperature setup for 1200°C temperature range.
3. The mass flow rate expected for the room temperature setup is 5 g/s and the expected flow rate for the high temperature setup is of 50-100 g/s.
4. A CFD model was developed to calculate the drag force reacting at a specified velocity. The design model from this study operates at air flow velocity of 30 m/s with a drag force of 24 N.
5. This prototype was designed to operate with both MFC and SMA; however, the SMA spring proved to be more efficient as a slow-moving product when actuated.

The importance of this project is to lead new development ideas for high temperature valves. Innovation increases the probabilities to react to changes and discover new opportunities. This project leads to new ideas that can be implemented to many different SOFC/GT hybrid system experiments, each of them serving a different project goal and helping achieve it.

5.1 Recommendations and Future Work

It is recommended that the MFC and SMA must be tested further ahead along with the built prototype. The final product will be tested at elevated temperatures (up to 1200℃), which is the similar temperature to experience at the Hyper Facility. Experimental verification must be developed to prove the reliability of the product. How the MFC can be used as a sensor instead of an actuator in the prototype must be analyzed as well. The design can be changed or improved in order to deliver a stronger valve mechanism for the hybrid system.

References

[1] Stephenson, D., & Ritchey, I. (1997). Parametric Study of Fuel Cell and Gas Turbine Combined Cycle Performance. *Volume 2: Coal, Biomass and Alternative Fuels; Combustion and Fuels; Oil and Gas Applications; Cycle Innovations*. doi: 10.1115/97-gt-340

[2] Veyo, S. E., Shockling, L. A., Dederer, J. T., Gillett, J. E., & Lundberg, W. L. (2002). Tubular Solid Oxide Fuel Cell/Gas Turbine Hybrid Cycle Power Systems: Status. *Journal of Engineering for Gas Turbines and Power*, *124*(4), 845–849. doi: 10.1115/1.1473148

[3] Valves Guide. (n.d.). Retrieved from http://www.wermac.org/valves/valves_general.html

[4] Shape-memory alloy. (n.d.). Retrieved from https://www.daido.co.jp/en/products/titanium/memory.html

[5] Macro Fiber Composite - MFC. (n.d.). *Macro Fiber Composite - MFC*. Retrieved from https://www.smart-material.com/media/Datasheets/MFC_V2.4-datasheet-web.pdf

[6] Kunzmann, J. (2007). Part 1: Analyzing the Fundamentals. *Development of an MFC Bending Element as an Actuator for Sensor Systems.*

[7] Bilgen, O., Kochersberger, K. B., Inman, D. J., & III, O. J. O. (2010). Macro-Fiber Composite actuated simply supported thin airfoils. *Smart Materials and Structures*, *19*(5), 055010. doi: 10.1088/0964-1726/19/5/055010

[8] Peponi, L., Navarro-Baena, I., & Kenny, J. (2014). Shape memory polymers: properties, synthesis and applications. *Smart Polymers and Their Applications*, 204–236. doi: 10.1533/9780857097026.1.204

[9] AbuJudom II, D.N., Thoma, P.E., Kao, M., Angst, D.R. (1992). *U.S. Patent No. 5,114,504.* Milwaukee, WI: Johnson Service Company.

[10] Nitinol Devices & Components. (n.d.). Shape Memory Nitinol Alloys* [Material Data Sheet]. Retrieved from https://confluentmedical.com/wp-content/uploads/2016/01/Material-Data-Sheet-Shape-Memory.pdf

[11] Fraser, D. B., & Warner, A. W. (1966). Lithium Niobate: A High-Temperature Piezoelectric Transducer Material. *Journal of Applied Physics*, *37*(10), 3853–3854. doi: 10.1063/1.1707937

[12] Summets, M. (2018). Chapter 1: Thin films of lithium niobate: potential applications, synthesis methods, structure and properties. In *Lithium Niobate-Based Heterostructures* (pp. 1–42). IOP Publishing Ltd.

[13] Burrows, S. E., Mcaughey, K. L., Edwards, R. S., & Dixon, S. (2012). High temperature thickness measurements using a bismuth titanate piezoelectric transducer. doi: 10.1063/1.4716329

[14] Lee, H., Zhang, S., Bar-Cohen, Y., & Sherrit, S. (2014). High Temperature, High Power Piezoelectric Composite Transducers. *Sensors*, *14*(8), 14526–14552. doi: 10.3390/s140814526

[15] Bilgen, O., Kochersberger, K. B., Inman, D. J., & Ohanian, O. J. (2010). Lightweight High Voltage Electronic Circuits for Piezoelectric Composite Actuators. *Journal of Intelligent Material Systems and Structures*, *21*(14), 1417–1426. doi: 10.1177/1045389x10381657

[16] Wang, Q.-M., & Cross, L. E. (1998). Performance analysis of piezoelectric cantilever bending actuators. *Ferroelectrics*, *215*(1), 187–213. doi: 10.1080/00150199808229562

[17] Top 10 Materials with the Highest Melting Point in the World. (2020, April 30). Retrieved from https://www.refractorymetal.org/list-of-metals-that-can-withstand-high-temperatures/

[18] Final Advanced Materials. (2020, April 24). Retrieved from https://www.final-materials.com/gb/209-high-temperature-adhesive

[19] Cheng, M., Whyte, D., & Lou, J. (2007). Numerical simulation of flow around a square cylinder in uniform-shear flow. *Journal of Fluids and Structures*, *23*(2), 207–226. doi: 10.1016/j.jfluidstructs.2006.08.011

[20] Risk at Work. (2020, April 24). Retrieved from https://www.hse.gov.uk/toolbox/ppe.htm

[21] Arizmendi, L. (2004). Review Article: Photonic applications of lithium niobate crystals. Physica Status Solidi (a). 201. 253-283. 10.1002/pssa.200303911.

[22] T.C. Waram, 2nd Edition, *Actuator Design Using Shape Memory Alloys,* T.C. Waram, Hamilton, Ontario, 1993.

[23] R.G. Gilberston, 3rd Edition, *Muscle Wires Project Book,* Mondo-tronics, Inc., San Anselmo, CA., 1994.

[24] T. Waram, "Design Principles for Ni-Ti Actuators," *Engineering Aspects of Shape Memory Alloys,* Butterworth-Heinemann Publishers, London, 1990, pp.234-244.

[25] Liang C, Rogers CA. Design of shape memory alloy springs with applications in vibration control. Journal of Intelligent Material Systems and Structures. 1997;4(2):229–242.

[26] Shigley JE. Mechanical engineering design. McGraw-Hill; 1972.

[27] Aguiar RAA, Neto WCDCL, Savi MA, Pacheco PMCL. Shape memory alloy helical springs performance: Modeling and experimental analysis. Materials Science Forum. 2013;758(2013):147–156.

[28] R.C. Juvinall, and K.M. Marshek, 2nd Edition, Fundamentals of Machine Component Design, John Wiley and Sons, Inc., NY, 1991, p.427-452.

[29] Wheeler, R. W., Benafan, O., Gao, X., Calkins, F. T., Ghanbari, Z., Hommer, G., … Turner, T. L. (2016). Engineering Design Tools for Shape Memory Alloy Actuators: CASMART Collaborative Best Practices and Case Studies. *Volume 1: Multifunctional Materials; Mechanics and Behavior of Active Materials; Integrated System Design and Implementation; Structural Health Monitoring*. doi: 10.1115/smasis2016-9183

[30] T. C. Waram, 2nd Edition, Actuator Design Using Shape Memory Alloys, T.C.Waram, Hamilton, Ontario, 1993.

[31] Follador, M., Cianchetti, M., Arienti, A., & Laschi, C. (2012). A general method for the design and fabrication of shape memory alloy active spring actuators. *Smart Materials and Structures*, *21*(11), 115029. doi: 10.1088/0964-1726/21/11/115029

[32] Koh J. S. (2018). Design of Shape Memory Alloy Coil Spring Actuator for Improving Performance in Cyclic Actuation. *Materials (Basel, Switzerland)*, *11*(11), 2324. https://doi.org/10.3390/ma11112324

[33] Cheng, S. S., Kim, Y., & Desai, J. P. (2017). Modeling and characterization of shape memory alloy springs with water cooling strategy in a neurosurgical robot. *Journal of intelligent material systems and structures*, *28*(16), 2167–2183. https://doi.org/10.1177/1045389X16685443

[34] Kong, Y., Bo, F., Wang, W., Zheng, D., Liu, H., Zhang, G., . . . Xu, J. (2019). Recent Progress in Lithium Niobate: Optical Damage, Defect Simulation, and On-Chip Devices. *Advanced Materials*, *32*(3), 1806452. doi:10.1002/adma.201806452

[35] Yang He, Hanxiao Liang, Rui Luo, Mingxiao Li, and Qiang Lin, "Dispersion engineered high quality lithium niobate microring resonators," Opt. Express 26, 16315-16322 (2018)

[36] Padoin, Eduardo, Fonseca, Jun Sergio Ono, Perondi, Eduardo André, & Menuzzi, Odair. (2015). Optimal Placement of Piezoelectric Macro Fiber Composite Patches on Composite Plates for Vibration Suppression. *Latin American Journal of Solids and Structures*, *12*(5), 925-947. doi.org/10.1590/1679-78251320

[37] Sun, X., Dai, Q., & Bilgen, O. (2018). Design and simulation of Macro-Fiber composite based serrated microflap for wind turbine blade fatigue load reduction. *Materials Research Express, 5*(5), 055505. doi:10.1088/2053-1591/aac318

[38] Rodrigue, H., Wang, W., Han, M., Kim, T. J., & Ahn, S. (2017). An Overview of Shape Memory Alloy-Coupled Actuators and Robots. *Soft Robotics, 4*(1), 3-15. doi:10.1089/soro.2016.0008

[39] Qian, H., Li, H., & Song, G. (2016). Experimental investigations of building structure with a superelastic shape memory alloy friction damper subject to seismic loads. *Smart Materials and Structures, 25*(12), 125026. doi:10.1088/0964-1726/25/12/125026

Appendix

Nomenclature

Symbol	Definition
τ	Shear Stress
F	Force
C	Spring Index
K	Wahl Correction Factor
d	Wire diameter
D	Average Diameter of the Spring
S	Stroke, Displacement
OD	Outer Diameter
ID	Inner Diameter
n	Number of Turns
γ	Strain
$\Delta\gamma$	Strain Difference
δ	Spring Deflection
G	Shear Modulus
R	Resistance
I	Current
P	Power
V	Voltage

Re	Reynolds Number
μ	Viscosity
$\dot{m}$	Mass Flow Rate
N	Newtons

Glossary

Final Valve Design

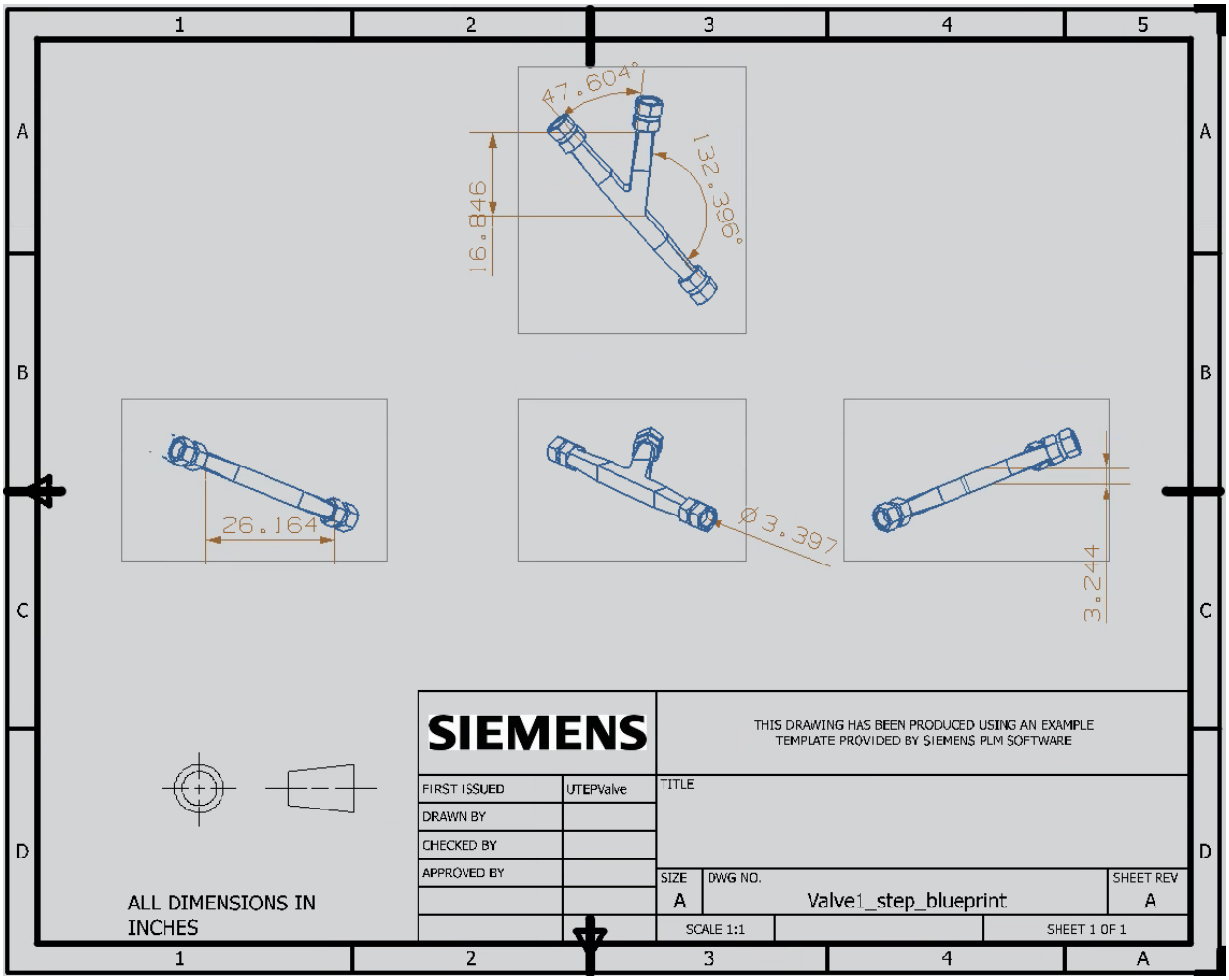

PIEZO MOUNT FOR LAB PROTOTYPE

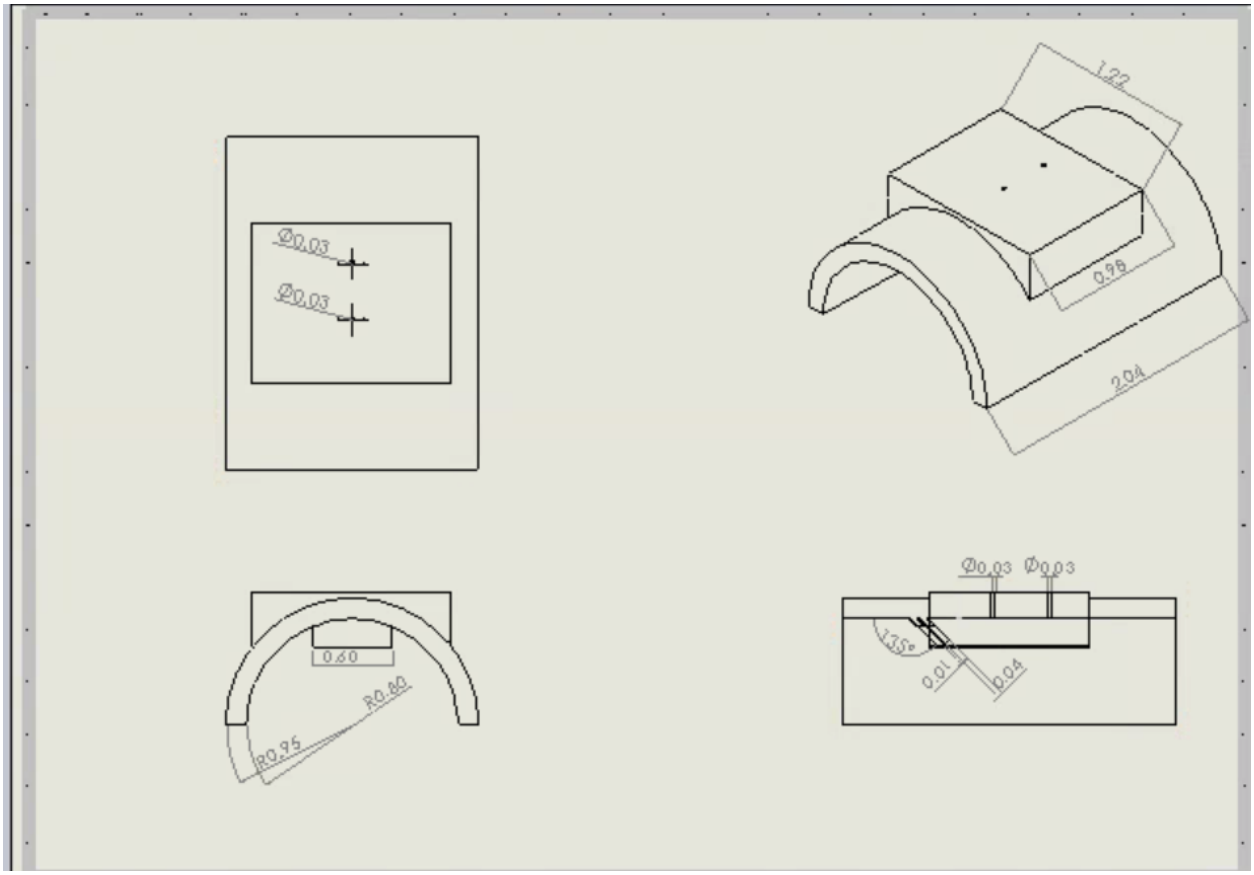

SHAPE MEMORY ALLOY INFORMATION

Type of Spring	Brand Name	Part Number/Ean	UNSPSC Code
1-Way SMA	Fuxus	3300058-5 (Part Number)	31160000
2-Way SMA	Nexmetal	0647732872286 (Ean)	-
1-Way SMA	Kellogg's Research Labs	NITI-SPR-CTL-100-ST (Part Number)	31161900

MACRO FIBER COMPOSITE INFORMATION

Brand Name	Model Name
Smart Material Corporation	M-2814-P1
Smart Material Corporation	M-4005-P1
Smart Material Corporation	M-2807-P1

Vita

Cynthia Morales received her Bachelor of Science from the University of Texas at El Paso in 2017. During her educational career, she had the opportunity to intern at the NASA Marshall Spaceflight Center conducting research in the propulsion department. She also interned with the Department of Energy at NETL where this thesis project started. While attending UTEP, she also conducted small satellite research for the Center for Space Exploration and Technology Research (cSETR). She has accepted a job offer to work at the Raytheon Missile Systems upon graduation as a thermal analyst engineer.